RSC Advances

PAPER

View Article Online
View Journal | View Issue

Cite this: *RSC Adv.*, 2026, **16**, 26506

Nanoantibiotics: peroxidase-mimicking bimetallic Au–Pt nanorods for antibacterial and antibiofilm applications

Nguyen Tran Truc Phuong, †[ab] Hanh An Nguyen, †[c] Kieu The Loan Trinh [de] and Thi Ngoc Diep Trinh *[f]

Conventional antibiotics, in spite of their wide application for centuries, are increasingly limited by the rapid evolution of bacterial resistance mechanisms that neutralize their therapeutic efficacy. To address this critical challenge, we report the development of a nanoantibiotic based on bimetallic gold–platinum nanorods (Au–PtNRs). The core–shell structure is formed by Pt nanodendrites covering the surface of Au nanorods, and the material's properties are determined through UV-vis, HRTEM, and EDS analyses. The synergistic effect of the Au core and Pt shell enhances enzyme-like activity, alters the electronic structure, and increases the stability and surface area compared to single-component materials. The synthesized Au–PtNRs exhibit effective antibacterial activity against Gram-negative *Salmonella* and Gram-positive *Enterococcus faecalis*. Notably, the material also possesses the ability to inhibit biofilm formation by bacteria. In this study, Au–PtNRs demonstrate high antibacterial potency, highlighting their potential as an alternative strategy to combat infectious bacteria. This work expands the application of functional nanomaterials in antimicrobial therapy and offers a promising approach for enabling human technological evolution to outpace bacterial adaptation.

Received 5th March 2026
Accepted 27th April 2026

DOI: 10.1039/d6ra01894g

rsc.li/rsc-advances

Introduction

Conventional antibiotics, despite their widespread use, face a fundamental limitation: bacteria evolve resistance faster than the rate at which new antibiotics can be developed.[1–3] A major reason lies in the reliance of such antibiotics on single-target biochemical inhibition, which is increasingly ineffective against bacteria capable of rapid adaptation.[4–6] Bacterial biofilms also cause great concern due to their high antibiotic-resistant characteristic. A biofilm is a surface-associated community of microorganisms playing a crucial role in microbial survival and adaptability.[7] Almost all bacteria are capable of forming biofilms. Biofilms help microorganisms enhance resistance to chemical and physical stresses such as unfavored temperatures and pH, UV radiation, nutrient shortage, and antimicrobial agents. Therefore, biofilms pose major health concerns due to their ability to resist disinfectants and antibiotics. To meet the actual demand, it is important to develop new materials that possess both antimicrobial and antibiofilm formation activities. Thus far, many materials with antimicrobial properties have been proposed. Nevertheless, there are limitations on research that focuses on new materials that can have both antimicrobial and antibiofilm activities.

Bimetallic nanoantibiotics emerge as a fundamentally different alternative to conventional antibiotics due to their unique physicochemical and catalytic properties.[8,9] Bimetallic nanoantibiotics are defined as nanostructured materials composed of two distinct metallic components that collectively induce antibacterial effects through non-specific, multi-modal stresses rather than single-target biochemical inhibition. These properties include synergistic electronic interactions, sustained catalytic activity, and shape-dependent physical membrane disturbance.[10–12] Peroxidase-like nanomaterials are among the most investigated enzyme-like materials. These materials catalyze the oxidation of various substrates using hydrogen peroxide. Because of their adjustable catalytic property and high resistance under many conditions, they have been widely applied in different fields, especially in antimicrobial and antibiofilm applications. Together, their features enable bimetallic nanoantibiotics to impose antibacterial stress through multiple concurrent pathways, including membrane disruption, redox imbalance, and biofilm destabilization.[13] As a result, bacteria exhibit a markedly reduced capacity to adapt to

[a]*NTT Hi-Tech Institute, Nguyen Tat Thanh University, Ho Chi Minh City, Vietnam*
[b]*Nguyen Tat Thanh University Center for Hi-Tech Development, Saigon Hi-Tech Park, Ho Chi Minh City, Vietnam*
[c]*Department of Molecular Biology, Institute of Food and Biotechnology, Can Tho University, Can Tho City, Vietnam*
[d]*Advanced Materials Technology Institute, Vietnam National University Ho Chi Minh City, Ho Chi Minh City 70000, Vietnam*
[e]*Vietnam National University, Ho Chi Minh City 70000, Vietnam*
[f]*Biotechnology Institute, Tra Vinh University, Vinh Long Province, Vietnam. E-mail: ttndiep@tvu.edu.vn*
† These authors contributed equally to this work.

bimetallic nanoantibiotics compared with conventional single-target antibiotics. Zhang *et al.* reported that gold–platinum (Au–Pt) nanodots exhibit remarkable antibacterial activity, achieving 97.1% inhibition of *Escherichia coli* (Gram-negative) and 99.3% inhibition of *Staphylococcus aureus* (Gram-positive).[14] However, their study did not evaluate the antibiofilm performance of these bimetallic Au–Pt nanomaterials, leaving an important aspect of their antimicrobial potential unexplored. Moreover, due to the isotropic geometry, spherical nanodots interact with the bacterial membrane through only a few discrete contact points, which restricts membrane disruption and ultimately weakens antibacterial performance.[15–17]

Leveraging insights from previous studies, the present work broadens the utility of bimetallic nanomaterials and addresses the inherent limitations of isotropic nanoparticle geometries through the synthesis of Au–Pt nanorods (Au–PtNRs). The bimetallic configuration harnesses the synergistic catalytic properties of Au and Pt, while the anisotropic rod-like morphology enhances the number and extent of contact sites with bacterial membranes. These combined attributes are anticipated to induce system-level failure in bacterial survival through multiple strategies, including membrane damage, oxidative imbalance, and biofilm destabilization.

Experimental

Materials and reagents

Gold(III) chloride solution ($AuCl_3 \cdot HCl$, 30% wt, 99.99%), silver nitrate ($AgNO_3$, 99.99%), hexadecyltrimethylammonium bromide (CTAB, 99%), sodium borohydride ($NaBH_4$, 98%), L-ascorbic acid (AA, 99%), sulfuric acid (H_2SO_4, ≥95%), potassium hexachloroplatinate (K_2PtCl_6, 99%), 3,3′,5,5′-tetramethylbenzidine (TMB, ≥99%), and hydrogen peroxide (H_2O_2, 3%) were acquired from Sigma-Aldrich Co., MO, USA. Sodium acetate (CH_3COONa, ≥99%), dimethyl sulfoxide (DMSO, 99.9%), and glacial acetic acid (CH_3COOH, 99.7%) were purchased from Fisher Ltd (UK). Deionized water used in the experiments was produced by a Milli-Q IQ 7000 purification system (Merck Millipore).

Fabrication of gold nanorods

Gold nanorods (AuNRs) were synthesized using a seed-mediated growth procedure, which is based on a modified method reported by Feng *et al.*[18] Briefly, the specific synthesis procedure is divided into two stages:

Preparation of the seed of gold nanoparticles (AuNPs): a mixture of CTAB (0.1 M) and $HAuCl_4$ (24 mM) was prepared in a 10 mL vial. Then, 0.6 mL of 0.01 M $NaBH_4$ was added to the vial and stirred at 400 rpm. The color of the solution gradually changed from yellow to light brown, indicating the formation of Au nuclei in the solution. The reaction was maintained for 2 h before the seed was used in the next step.

Growth of AuNRs: a mixture of CTAB (100 mL, 0.1 M), $HAuCl_4$ (2.04 mL, 0.024 M), H_2SO_4 (2 mL, 0.5 M), $AgNO_3$ (1 mL, 10 mM), and AA (800 μL, 0.1 M) was prepared in a glass vessel with a lid. Then, 240 μL of the seeds was added to the mixture to provide nucleation sites for the anisotropic growth of AuNPs, assisted by CTAB and $AgNO_3$. After 16 h, the solution mixture was washed three times with DI water by centrifugation at 12000 rpm. Finally, the solid obtained was dispersed in 50 mL of DI water and stored at 4 °C in the dark for subsequent analysis.

Fabrication of bimetallic Au–Pt NRs

The Pt shell was grown on the AuNRs according to the following process: 2.34 mL of K_2PtCl_6 (2 mM) was added to a glass flask containing 10 mL of AuNRs. Then, AA was added dropwise into the mixture, maintaining the molar ratio of AA : K_2PtCl_6 at 10 : 1. The solution was adjusted to a final volume of 30 mL with DI water before being placed in a 60 °C water bath for 16 h. The formation of the Pt layer on the Au rods resulted in a color shift of the solution from orange-red to deep blue. The Au–PtNRs obtained were purified by centrifugation at 12000 rpm three times, then redispersed in 30 mL of DI water and stored in the dark at 4 °C. The step-by-step synthesis process is depicted in Fig. 1.

Instrument characterization

A Cary 60 UV-Vis spectrophotometer (Agilent Technologies, Inc., USA) was used to evaluate the optical properties and enzyme-like activity of Au–PtNRs in the absorption mode within the wavelength range of 300–800 nm at a scanning speed of 400 nm min^{-1}. The size distribution of Au–PtNRs was evaluated by dynamic light scattering (Zetasizer Advance Series–Ultra, Malvern Panalytical Ltd). The structure and morphology of Au–PtNRs were characterized using transmission electron microscopy (HRTEM, JEM-2100, JEOL). Energy-dispersive X-ray

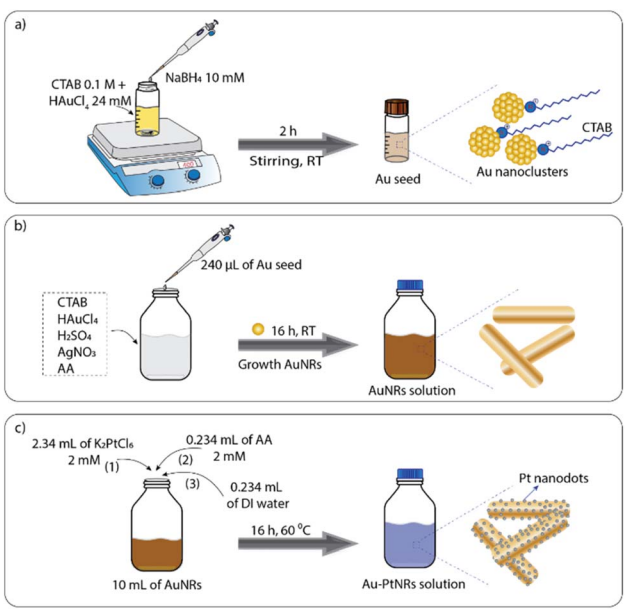

Fig. 1 (a) A schematic illustration of the Au seed preparation process. (b) A schematic illustration of AuNR growth. (c) A schematic illustration of the Au–PtNR material fabrication.

spectroscopy (EDX, JEOL JEM 2010) was employed to determine the elemental composition of the bimetallic Au–PtNRs.

Enzyme-mimicking activities of bimetallic Au@Pt NRs

The peroxidase-like (POD-like) activity of Au–PtNRs was evaluated against the TMB substrate under H_2O_2-containing and -free conditions. Typically, systems consisting of 1 mL of NaAc buffer (pH = 5), 200 μL of TMB (10 mM), and 100 μL of the Au–PtNRs solution were prepared in an Eppendorf tube. Then, 20 μL of H_2O_2 was added to the mixture and mixed thoroughly using a vortex mixer. The same preparation was performed for the system containing AuNRs. The UV-Vis absorption spectra were recorded in the wavelength range of 400–800 nm to determine the POD-like activity of AuNRs and Au–PtNRs. Additionally, the H_2O_2/TMB system in NaAc buffer was employed to assess the sensitivity of Au–PtNRs to H_2O_2. Firstly, 100 μL of the Au–PtNRs solution was mixed with 200 μL of TMB (10 mM) and 1 mL of NaAc buffer. Then, 20 μL of H_2O_2 with different concentrations (10–100 mM) was added. The absorbance at 652 nm was recorded every 30 s for 300 s and was plotted according to the Michaelis–Menten enzyme kinetics. To characterize the oxidase-like (OXD-like) activity of Au–PtNRs, an AA solution (5 mM) was mixed with Au–PtNRs at a ratio of 80 μL of AA, 300 μL of the Au–PtNRs solution, and 2.5 mL of DI water at room temperature for 60 min under normoxic/hypoxic conditions. Finally, the absorption spectrum of the solution was recorded in the 200–300 nm region to evaluate the decrease of AA concentration.

Bacterial strains and growth media

Two types of bacteria, *Salmonella* and *Enterococcus faecalis* (*E. faecalis*), were employed in this study. Bacteria were grown in Luria-Bertani broth (LB) at 37 °C with shaking. Mueller–Hinton agar (MHA) was also employed for plate culturing.

Antibacterial activity test

To test the antibacterial activity of the materials, a bacterial suspension (McFarland 0.5 Turbidity Standard) was prepared and spread on MHA media separately. Then, materials were placed onto the inoculated agar plates. The plates were incubated at 37 °C overnight. At last, the diameters of the inhibition zones were measured to evaluate the antibacterial activity of the materials. Each experiment was repeated three times in parallel.

Effect of the Au–PtNR concentration on bacterial growth

The Au–PtNRs at different concentrations, including two-fold, four-fold, eight-fold, and sixteen-fold dilutions, were employed to test the effect of the concentration of the materials on bacterial growth. To observe bacterial growth inhibition in liquid media, a bacterial suspension was cultured using LB media. The materials at different concentrations were added to each culturing vial. The bacterial suspension in LB media without Au–PtNRs was used as the positive control. The suspension was incubated at 37 °C overnight. The results were interpreted by measuring absorbance at 600 nm. To observe bacterial growth inhibition on agar plates, a bacterial suspension (McFarland 0.5 Turbidity Standard) was prepared and spread on MHA media separately. Then, the materials at different concentrations were placed onto the inoculated agar plates. The plates were incubated at 37 °C overnight. At last, the diameters of the inhibition zones were measured to evaluate the antibacterial activity of the materials. In this experiment, the lowest concentration of the material that inhibited bacterial growth was determined.

Antibiofilm formation activity test

A bacterial suspension (McFarland 0.5 Turbidity Standard) was placed into a tube containing liquid media and then incubated at 37 °C for 24 h without agitation to permit biofilm formation. Crystal violet staining was used to assess antibiofilm formation activity. The solution was then carefully removed from the incubated tube. The attached cells were softly washed to remove any unbound factors. Crystal violet was used to stain the biofilm that remained attached to the tube. Absorbance at 570 nm was determined.

Results and discussion

Characterization of bimetallic Au–PtNRs

The characteristic optical properties of AuNRs and Au–PtNRs materials were evaluated through UV-Vis absorption spectra in the range from 300 to 800 nm (Fig. 2a). In the case of AuNRs, a strong absorption peak was observed in the visible region at 516 nm and a strong absorption peak was observed in the near-infrared region at 730 nm, corresponding to the longitudinal and transverse modes characteristic of the rods, respectively, which were previously reported by Liu *et al.*[19] Meanwhile, the Au–PtNRs sample exhibited the complete quenching of the plasmon peak in the visible region of AuNRs, which was caused by the formation of Pt nanodots and covering of a thick layer of Pt nanodots on the AuNRs surface.[18] In fact, the DLS analysis results (Fig. 2b) also showed the size distribution in two different regions: around 20 nm (peak 1), corresponding to the diameter, and around 100 nm (peak 2), corresponding to the length of the nanorods.

The HRTEM images shown in Fig. 3a revealed the morphologies, structures, and sizes of the Au–PtNRs sample, which were consistent with the results of UV-Vis and DLS

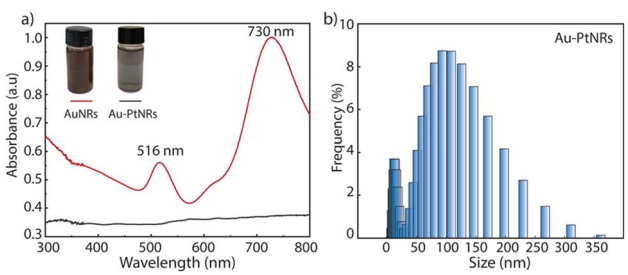

Fig. 2 (a) UV-vis spectrum and (inset) images of the solution and (b) DLS spectrum of the bimetallic Au–PtNRs.

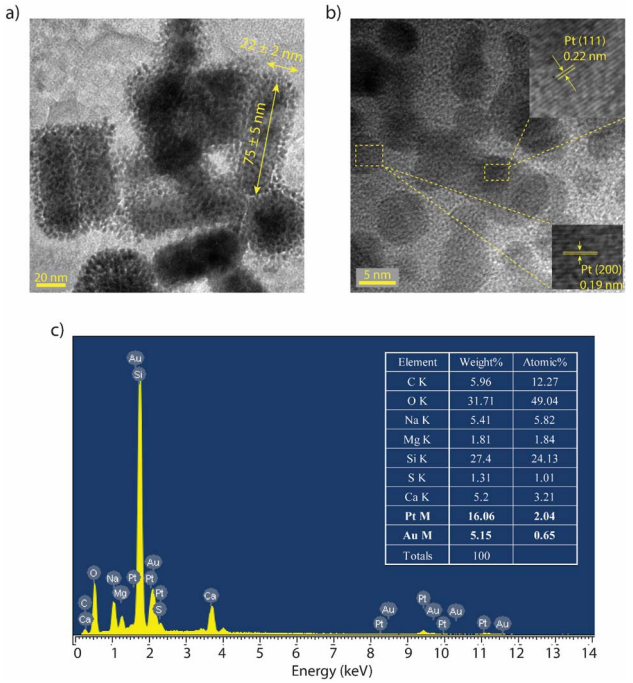

Fig. 3 (a and b) HRTEM images and (c) EDS spectrum of the bimetallic Au–PtNR material.

analyses. In detail, the Au–PtNRs had a core–shell structure with a rod length of about 75 ± 5 nm and a diameter of 22 ± 2 nm. The Pt nanodots were evenly attached to the surface of the Au rod, forming a relatively porous shell with a thickness of approximately 5.5 ± 0.5 nm, which causes the plasmon quenching of AuNRs in the UV-vis spectrum. In addition, *d*-spacing analysis from HRTEM images in the shell region of the Au–PtNRs material (Fig. 3b) provided evidence of the formation of a Pt nanodot shell on AuNRs, with the determined *d*-spacings of 0.22 and 0.19 nm, corresponding to the characteristic (111) and (200) lattice planes of Pt, respectively. By contrast, the elemental composition of the Au–PtNRs sample, as determined by EDX analysis (Fig. 3c), also revealed the presence of Au and Pt components with ratios of 5.15 and 16.06 wt%, respectively, confirming the successful synthesis of the bimetallic Au–PtNRs material.

Enzyme-like activity

The catalytic ability of Au–PtNRs to oxidize the TMB substrate by consuming H_2O_2 (POD) is shown in Fig. 4a. The color change from colorless to blue, accompanied by the appearance of an absorption peak at 650 nm, characteristic of oxTMB in the Au–PtNRs/TMB/H_2O_2 system, demonstrated that Au–PtNRs possessed POD-like activity at room temperature. Furthermore, compared with single-component AuNRs, Au–PtNRs showed superior catalytic activity (under the catalytic test condition for 30 min at room temperature). The synergistic effect of the two metals, Au and Pt, causing changes in the electronic properties and adsorption capacity, was one of the reasons leading to the enhancement in the POD-like activity of Au–PtNRs.[20] By contrast, the core–shell structure with a porous Pt nanodot layer covering the surface of AuNRs helped increase the catalytic surface area and H_2O_2 adsorption capacity, which also enhances the POD-like activity of Au–PtNRs.[21] Michaelis–Menten steady-state kinetics (Fig. 4b) and Lineweaver–Burk plots (Fig. 4c) were constructed to determine the rate of oxidation of TMB to oxTMB with changes in the H_2O_2 concentration, based on the maximum absorbance of TMB at 650 nm. The Michaelis constant (K_{max}) and maximal reaction velocity (V_{max}) of Au–PtNRs were calculated to be 82.31 and 8.53 × 10^{-7} M min^{-1}, respectively. The OXD-like activity of Au–PtNRs was also investigated based on the decrease in the ascorbic acid substrate concentration observed using the absorbance at 260 nm (Fig. 4d). Under both normoxic and hypoxic conditions, the characteristic absorption peak of ascorbic acid was observed to decrease in intensity at 60 min of investigation. Notably, under normoxic conditions, the absorption intensity at 260 nm decreased by 21.72%, which was 1.75 times higher than that under hypoxic conditions, with a decrease of 12.37%. This provides evidence of the OXD-like activity of Au–PtNRs.

Antibacterial activity

Bimetallic Au–PtNRs have recently gained significant attention as they have been extensively employed to combat pathogenic bacteria. The antibacterial activity of the Au–PtNRs was tested against two types of bacteria, namely, Gram-negative *Salmonella* and Gram-positive *E. faecalis*. First, materials in an aqueous solution were directly added to MHA plates incubated with pathogenic bacteria. The formation of the inhibition zone was observed by monitoring the visible halos on the agar plates. A bigger diameter of the inhibition zone represents greater effectiveness in antibacterial activity. The results indicated the antibacterial activity of the Au–PtNRs on both Gram-negative and Gram-positive bacteria (Fig. 5a). Several mechanisms have been proposed to demonstrate the mode of action of the materials (Fig. 5b). Cell membrane damage, reactive oxygen species (ROS) generation and oxidative stress, DNA damage, protein denaturation, and protein synthesis inhibition are the main mechanisms of antibacterial activity of bimetallic nanozymes. The inhibition of bacterial growth is accomplished by one or a combination of the above mechanisms. Among these mechanisms, peroxidase-like activity plays a key antibacterial role, as it can generate large amounts of ROS. In general, the bimetallic Au–PtNRs possess antibacterial activity mainly thanks to their ability to produce ROS, such as hydrogen peroxide, hydroxyl radicals, singlet oxygen, and superoxide anions, which are highly toxic to bacteria. ROS can be spontaneously produced through their peroxidase-like characteristics. When ROS are in contact with bacterial cells, oxidative stress reactions occur, which result in lipid membranes' peroxidation and the oxidation of cellular substances such as proteins and nucleic acids, thereby causing irreversible damage to the integrity of bacterial cells and cell functions.[22] Moreover, natural enzymes are usually susceptible to environmental factors like pH, inhibitors, and temperature, leading to their low stability, requirement of crucial conditions for storage, and

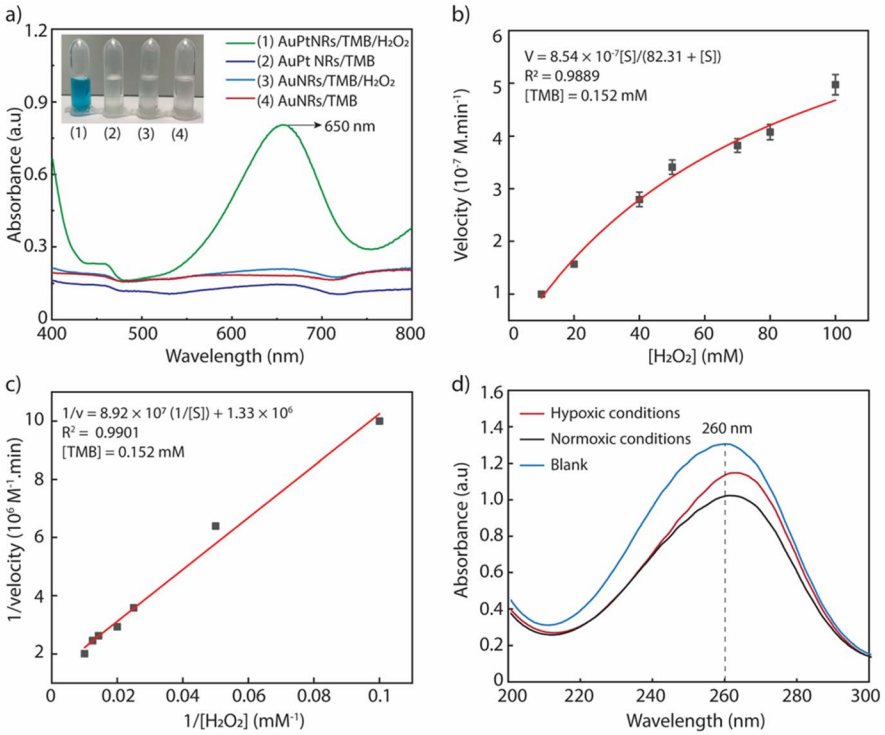

Fig. 4 (a) UV-vis absorption spectrum and color changes of the AuNRs/TMB and Au–PtNRs/TMB systems in the presence or absence of H_2O_2. (b and c) Michaelis–Menten fitting curve and Lineweaver–Burk fitting of the ·OH generation velocity by Au–PtNRs against the H_2O_2 concentration, respectively. (d) UV-vis absorption spectrum of the Au–PtNRs/AA system under normoxic and hypoxic conditions.

high production cost, which ultimately limit their use in controlling infectious diseases.[23] Meanwhile, our developed materials are stable and easy to prepare, handle, store, and transport under various conditions such as temperature, pH, and salt concentration. For these reasons, the peroxidase-mimicking bimetallic Au-PtNRs can serve as a potential alternative for effectively removing pathogenic bacteria. This observation is consistent with the results shown in Fig. 4, where the peroxidase activity of Au–PtNRs is demonstrated.

Effect of the Au–PtNRs concentration on bacterial growth

Fig. 6 shows the effect of Au–PtNRs at different concentrations on bacterial growth. First, different concentrations of Au–PtNRs in an aqueous solution, including an initial concentration of 74 μg mL^{-1} and 2-, 4-, 8-, and 16-fold dilutions, were directly dropped on pathogenic bacteria spread on MHA plates, and the appearance of an inhibition zone was monitored. Interestingly, concentrations of 2- and 4-fold dilutions of Au–PtNRs, which are 37 and 18.5 μg mL^{-1}, respectively, formed visible inhibition

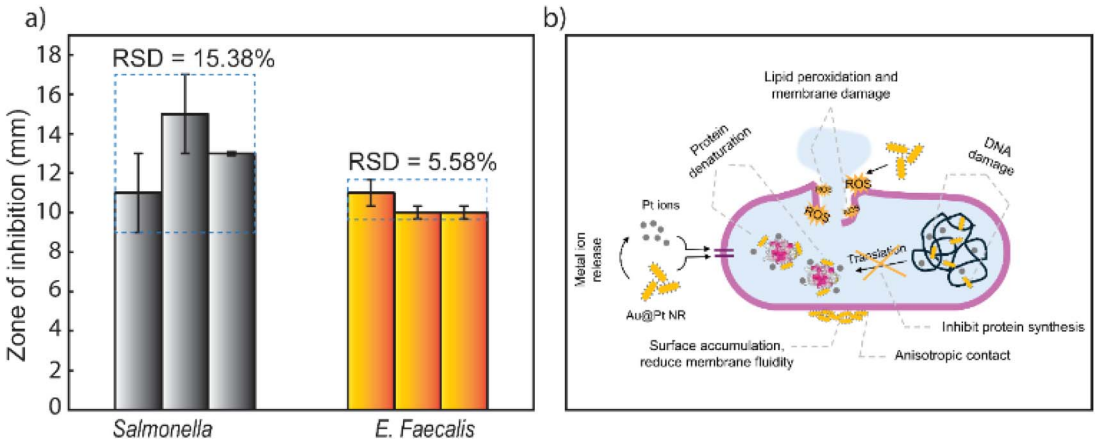

Fig. 5 (a) Results showing the antibacterial activity of Au–PtNRs against *Salmonella* and *E. faecalis*. (b) Some possible mechanisms of the antibacterial activity.

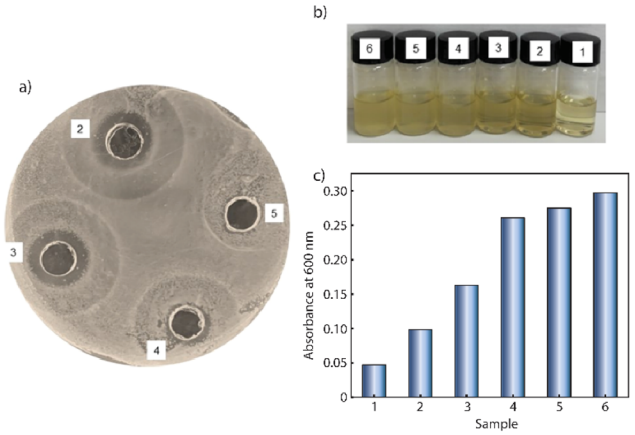

Fig. 6 Effect of the material concentration on bacterial growth. (a) Bacterial growth on an agar plate. (b) Bacterial growth in a solution. (c) Absorbance of the bacterial suspension at 600 nm.

halos on the Gram-negative bacteria *Salmonella* (Fig. 6a). As shown in Fig. 6b, we then determined the antibacterial effect of Au–PtNRs at different concentrations on the growth of bacteria in solutions. In agreement with the results obtained on the solid medium, concentrations of 2- and 4-fold dilutions of Au–PtNRs successfully inhibited bacterial growth, as evidenced by the dramatic drop in absorbance at 600 nm (Fig. 6c). In all, these results show that the Au–PtNRs have bactericidal activities against pathogenic bacteria. From these results, we can conclude that at a concentration of 18.5 μg mL^{-1}, Au–PtNRs can successfully inhibit the growth of bacteria.

Antibiofilm formation activity

The public health community has recognized biofilms as an important source of pathogens due to their vital roles in infectious diseases such as periodontitis and chronic diseases. In addition, nosocomial infections are often caused by opportunistic pathogens forming biofilms, which generally spread through surgical site infections, urinary tract infections, invasive medical devices, and surfaces of medical equipment, such as gloves, door knobs, and bed sheets. To evaluate the ability of bimetallic Au–Pt NRs to inhibit biofilm formation, antibiofilm formation tests were carried out. Fig. 7a shows antibiofilm formation test results. Crystal violet staining exhibited the ability to form a biofilm of *E. faecalis*, an opportunistic bacterium capable of causing infections, especially in the nosocomial environment. Treatment with ampicillin was selected, and treatment without ampicillin or bimetallic Au–PtNRs acted as the positive control. In the positive control, without any inhibitors, bacteria grew and formed a strong biofilm, which was indicated by the highest absorbance at 570 nm. In the ampicillin treatment, a dramatic drop in absorbance was observed, which proved that the antibiotic could inhibit biofilm formation. Ampicillin can be effective, particularly toward the susceptible *E. faecalis* strain used in this study, mainly by disrupting cell wall synthesis, therefore affecting the structural

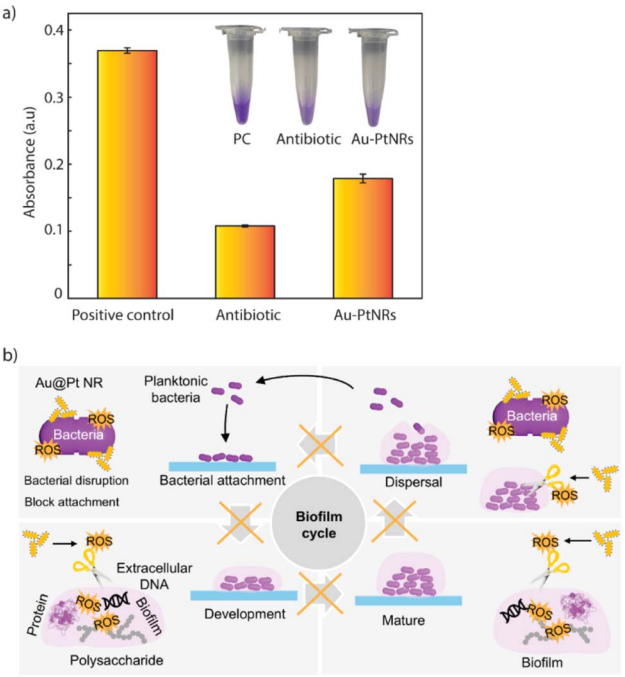

Fig. 7 (a) Results showing the antibiofilm effect of Au–PtNRs against *E. faecalis*. (b) Schematic of the biofilm cycle.

integrity of the biofilm. Similarly, when bimetallic Au–PtNRs were applied to the bacterial suspension, the formation of the biofilm was successfully decreased, as indicated by the drop in absorbance at 570 nm. Compared to that in the positive control, the biofilm of *E. faecalis* in bimetallic Au–Pt nanozyme treatment was successfully removed. The peroxidase-like nature of the material is considered to hold great potential for antibiofilm formation. The material can cause bacterial disruption, which blocks bacterial attachment, therefore preventing biofilm development. Moreover, the peroxidase-like activity oxidatively cleaves the biofilm components, including extracellular DNA, proteins, and polysaccharides, which leads to biofilm elimination.[23] These results further confirm the excellent antibacterial effect of bimetallic Au–PtNRs, which disrupt the biofilm. Although the antibiofilm formation of bimetallic Au–PtNRs is weaker than that of the antibiotic, the potential of the material is still very promising. This is because ampicillin prevents the formation of the bacterial biofilm mainly by attacking the synthesis of the bacterial cell wall. Meanwhile, the proposed material possesses peroxidase-like activity, which has combined effects on the bacteria and their ability to form biofilm, as shown in Fig. 7b. This can benefit from bacteria on which ampicillin has no effect. Further study on different bacteria with a resistant nature can be conducted to clarify the advantages of our material.

Conclusions

To overcome the remaining challenges of conventional antibiotics, we developed a nanoantibiotic based on bimetallic Au–PtNRs by chemical reduction. With a structure consisting of Au

nanorods approximately 69.5 ± 5 nm in length serving as the core, covered by Pt dendrites approximately 5.5 ± 0.5 nm in thickness, Au–PtNRs demonstrate high antimicrobial efficacy due to the synergistic effect of the two materials (Au and Pt). Specifically, the prepared Au–PtNRs exhibit pronounced antibacterial activity against Gram-negative *Salmonella* and Gram-positive *E. faecalis*, yielding significant antibacterial outcomes. Systematic investigations reveal that Au–PtNRs possess strong antibacterial efficacy, underscoring their promise as an alternative strategy for combating antibiotic-resistant bacteria. Moreover, to the best of our knowledge, the antibiofilm formation activity of Au–PtNRs was evaluated for the first time in this study and indicated the potential of this material for antimicrobial studies. This study broadens the scope of functional nanomaterials in antimicrobial applications and presents a potential pathway for advancing antimicrobial technologies beyond bacterial adaptation.

Author contributions

Nguyen Tran Truc Phuong: conception, investigation, data curation, methodology, visualization, writing – original draft preparation. Hanh An Nguyen: conception, investigation, data curation, visualization, writing – original draft preparation. Kieu The Loan Trinh: conception, investigation, data curation, visualization, writing – original draft preparation. Thi Ngoc Diep Trinh: methodology, resources, supervision, visualization, writing – review and editing.

Conflicts of interest

There are no conflicts to declare.

Data availability

The authors confirm that the data supporting the findings of this study are available within the article.

Acknowledgements

This research received no external funding. We acknowledge the support of time and facilities from Tra Vinh University (TVU) for this study. We also acknowledge Nguyen Tat Thanh University, Ho Chi Minh City, Vietnam, for supporting this study.

References

1 E. Bakkeren, M. Diard and W. D. Hardt, *Nat. Rev. Microbiol.*, 2020, **18**, 479–490.
2 L. Boeck, *Curr. Opin. Microbiol.*, 2023, **74**, 102328.
3 D. N. Wilson, V. Hauryliuk, G. C. Atkinson and A. J. O'Neill, *Nat. Rev. Microbiol.*, 2020, **18**, 637–648.
4 A. Sett, V. Dubey, S. Bhowmik and R. Pathania, *ACS Infect. Dis.*, 2024, **10**, 2525–2539.
5 M. W. Van Goethem, R. Marasco, P. Y. Hong and D. Daffonchio, *Microb. Biotechnol.*, 2024, **17**, e14430.
6 S. Sun and X. Chen, *World J. Microbiol. Biotechnol.*, 2024, **40**, 295.
7 K. Sauer, P. Stoodley, D. M. Goeres, L. Hall-Stoodley, M. Burmølle, P. S. Stewart and T. Bjarnsholt, *Nat. Rev. Microbiol.*, 2022, **20**, 608–620.
8 H. Lin, Y. Liu, J. Deng, L. Jing, Z. Wang, L. Wei, Z. Wei, Z. Hou, J. Tao and H. Dai, *Environ. Sci.: Adv.*, 2025, **4**, 33–56.
9 V. Bachhar, V. Joshi, A. Bhatia, T. Rom, M. Duseja and R. K. Shukla, *J. Environ. Chem. Eng.*, 2025, **13**, 116829.
10 M. Larrañaga-Tapia, B. Betancourt-Tovar, M. Videa, M. Antunes-Ricardo and J. L. Cholula-Díaz, *Nanoscale Adv.*, 2023, **6**, 51–71.
11 H. Ma, W. Zhang, K. Yang, Z. Liu and W. Zhang, *J. Environ. Manage.*, 2025, **376**, 124465.
12 D. S. Idris and A. Roy, *J. Inorg. Organomet. Polym. Mater.*, 2023, **34**, 1055–1067.
13 R. Sheng Li, J. Liu, C. Wen, Y. Shi, J. Ling, Q. Cao, L. Wang, H. Shi, C. Z. Huang and N. Li, *Sci. Adv.*, 2023, **9**, eadg9601.
14 S. Zhang, Q. Lu, F. Wang, Z. Xiao, L. He, D. He and L. Deng, *ACS Appl. Mater. Interfaces*, 2021, **13**, 37535–37544.
15 F. Y. Rezaei, G. Pircheraghi and V. S. Nikbin, *ACS Appl. Nano Mater.*, 2024, **7**, 15242–15254.
16 J. Ma, K. Li and S. Gu, *RSC Adv.*, 2022, **12**, 4852–4864.
17 M. Xu, Y. Song, J. Wang and N. Li, *View*, 2021, **2**, 20200154.
18 L. Feng, X. Wu, L. Ren, Y. Xiang, W. He, K. Zhang, W. Zhou and S. Xie, *Chem.–Eur. J.*, 2008, **14**, 9764–9771.
19 J. B. Liu, L. Long, Y. S. Zhang, Y. P. Wang, F. S. Liu, W. Y. Xu, M. J. Zong, L. Ma, W. Q. Liu, H. Zhang, J. Yan, J. Q. Chen, Y. L. Ji and X. C. Wu, *Front. Phys.*, 2015, **11**, 118501.
20 H. J. Lee, D. Hanyu, A. T. N. Dao and K. Kaneko, *Sci. Rep.*, 2025, **15**, 29474.
21 Y. Zhuang, H. Yin, Y. Huang, F. Jiang, L. Li, Z. Wu, Y. Yang, X. Cao and W. Wei, *Biosens. Bioelectron.*, 2025, **283**, 117536.
22 F. Gao, T. Shao, Y. Yu, Y. Xiong and L. Yang, *Nat. Commun.*, 2021, **12**, 745.
23 G. Fang, R. Kang, S. Cai and C. Ge, *Nano Today*, 2023, **48**, 101755.